CLM-P891

CLM-P891

An Improved Mathematical Model of Melt/Water Detonations, Part I: Model Formulation and Example Results

D. F. Fletcher

CULHAM LABORATORY

AEA TECHNOLOGY

CLM-P891

An Improved Mathematical Model of Melt/Water Detonations, Part I: Model Formulation and Example Results

D.F. Fletcher

Culham Laboratory, Abingdon, Oxon., OX14 3DB

ABSTRACT

In this paper an improved mathematical model of melt/water detonations is described. The model has been developed to study the escalation and propagation stages of a vapour explosion. The modelling presented in this paper represents a significant extension of an earlier version of the CULDESAC code [1], also developed at Culham Laboratory. After describing the physics of this problem, a complete description of the conservation equations and constitutive relations which form the model is given. The solution procedure is then described and some results from example simulations are presented. These results demonstrate the improved performance of the new model and illustrate the effect of the initial mixture void fraction on propagation. The rôle played by various solution parameters and constitutive physics assumptions is also examined. Part II of this paper [2] contains a detailed study of the escalation stage.

March, 1990

Contents

Nomenclature

A	area factor
b_0	coefficient in the artificial viscosity formula
c_d	drag coefficient
c_{frag}	constant in the fragmentation model
c_v	specific heat at constant volume
e	internal energy
e_s	stagnation energy
h	heat transfer coefficient
h_s	stagnation enthalpy
K	momentum exchange function
L	length-scale
p	pressure
R	energy exchange function
T	temperature
t	time
V	velocity
x	axial coordinate

Greek Symbols

α	volume fraction or void fraction
ρ	density
μ_a	artificial viscosity
Γ_f	mass transfer rate
Γ_{frag}	length-scale source term
Δt	space step
Δx	time step

Subscripts

e	effective fluid (water plus fragments)
f	fragments
m	melt droplets
w	water

1 Introduction

If a hot liquid (melt) contacts a cooler volatile liquid, in some circumstances the energy transfer rate can be so rapid and coherent that an explosion results. Such explosions are a well-known hazard in the metal casting industry [3], in the transportation of liquefied natural gas over water [4], in the paper industry where a molten salt (called smelt) may contact water [5], and it is postulated that they may occur in submarine volcanisms [6]. They are also studied in the nuclear industry, to assess the consequences of the unlikely event that in a severe accident molten material contacts residual coolant and such an explosion results [7].

It is postulated that explosions of this type progress through a number of distinct phases [7]. Initially, the melt and water mix on a relatively slow timescale ($\sim$1 second). During this stage the melt and water zones have a characteristic dimension of the order of 10mm. Because of the high temperature of the melt a vapour blanket insulates the melt from the water and there is relatively little heat transfer. If this vapour blanket is collapsed in some small region of the mixture, high heat transfer rates result and there is a rapid rise in the pressure locally. In some circumstances this pressure pulse can cause further vapour film collapse, so that it escalates and propagates through the mixture, causing coherent energy release. The propagating pressure pulse (which steepens to form a shock wave) has two main effects. Firstly, it collapses the vapour blanket, initiating rapid heat transfer. Secondly, it causes differential acceleration of the melt and water, which in turn leads to relative velocity breakup of the melt and a large increase in the melt surface area. As the energy of the melt is rapidly transferred to the water high pressure steam is produced, which expands, with the potential to cause damage to any surrounding structures.

The analogy between thermal detonations and classical chemical detonations was first postulated in 1975 [8]. Since that time a number of steady-state and transient models have been developed to study vapour explosions. These are all based on the analogy between chemical and thermal detonations. They have recently been reviewed by Fletcher and Anderson [9], who concluded that the current generation of models are not yet able to simulate many of the complex physical phenomena occurring in a thermal detonation, but that they provide a useful tool capable of stimulating experimental research.

This paper contains a description of the improvements which have been made to an earlier version of a model, called CULDESAC, developed by Fletcher and Thyagaraja [1, 10]. Results obtained with the early version of the model showed that:

(a) for very high heat transfer rates propagation occurs in highly voided mixtures [1];

(b) the presence of a permanent gas does not affect the propagation behaviour significantly for high heat input rates [10];

(c) mixture inhomogeneities can lead to complicated propagation behaviour [11];

(d) for a lower heat transfer rate a detonation may take a considerable time to develop in a spherical geometry whereas it develops rapidly in a planar geometry [11].

This work highlighted the need to make the model sufficiently flexible that it could be applied over a wide range of initial void fractions and to low heat input rates. This was prevented in the earlier version of the model by the appearance of high frequency oscillations at the shock front, in simulations where the compressibility of the material behind the front was low.

The new version of the model presented in this paper achieves the aim stated above. In addition, an extra velocity field has been included so that the melt particles formed by the fragmentation process are no longer required to move with the water velocity, as is the case in all previous models [9]. Section 2 of this paper contains a description of the partial differential equations which make up the model and the constitutive relations used to close it. The new solution procedure, developed to enable strong shocks to be captured using artificial viscosity, is described in section 3. Section 4 contains the results from some simulations which show that the new solution scheme does indeed perform well. These results are used to illustrate how the model can be used to make predictions in advance of experimental data. Section 5 contains the conclusions.

2 Description of the Model

In this section the partial differential equations and constitutive relations which constitute the model are described. The model is transient and one-dimensional, although this may be planar, cylindrical, spherical or any user-specified slowly varying shape. (This is achieved by making suitable choices for the area factors, A, in the equations given below.) The mixture is assumed to consist of melt droplets, water and steam. Behind the detonation front the droplets are fragmented by boundary layer stripping and the water is heated by energy transfer from the fragments. This situation is shown schematically in figure 1.

In the model this situation is represented using three different components, namely melt droplets (m), melt fragments (f) and water (w). In order to restrict the number of constitutive relations required to close the model, the simplifying assumption that steam and water are always in mechanical and thermal equilibrium is made. This assumption is justified once supercritical temperatures and pressures occur and provides a first approximation for subcritical conditions. Each species is assumed to have its own velocity field. The fragmentation process is assumed to be boundary layer stripping [12], although the model is sufficiently general to apply to any hydrodynamic fragmentation process. Heat is transferred from the fragments to *all* of the water at a finite rate. Thus no allowance is made for local thermal disequilibrium, around the fragments, in the water phase.

This problem has been formulated mathematically using the usual multiphase flow equations [13], where the presence of each species is specified by a volume fraction and all of the species are at a common pressure. The simplifying assumption that the melt and fragments are incompressible is made, so that $\rho_f = \rho_m = \text{constant}$.

2.1 Conservation Equations

Conservation of mass applied to the water, melt and fragments gives

$$\frac{\partial}{\partial t}(\alpha_w \rho_w) + \frac{1}{A}\frac{\partial}{\partial x}(A\alpha_w \rho_w V_w) = 0, \tag{1}$$

$$\frac{\partial}{\partial t}(\alpha_m \rho_m) + \frac{1}{A}\frac{\partial}{\partial x}(A\alpha_m \rho_m V_m) = -\Gamma_f \tag{2}$$

and

$$\frac{\partial}{\partial t}(\alpha_f \rho_m) + \frac{1}{A}\frac{\partial}{\partial x}(A\alpha_f \rho_m V_f) = \Gamma_f. \tag{3}$$

In equations (2) and (3) Γ_f is the mass transfer rate due to fragmentation and is specified later.

Conservation of momentum for the water, melt and fragments gives

$$\frac{\partial}{\partial t}(\alpha_w \rho_w V_w) + \frac{1}{A}\frac{\partial}{\partial x}(A\alpha_w \rho_w V_w^2) =$$

$$-\alpha_w \frac{\partial p}{\partial x} + \frac{\partial}{\partial x}\left(\alpha_w \mu_a \frac{1}{A}\frac{\partial}{\partial x}(AV_w)\right) + K_{mw}(V_m - V_w) + K_{fw}(V_f - V_w), \tag{4}$$

$$\frac{\partial}{\partial t}(\alpha_m \rho_m V_m) + \frac{1}{A}\frac{\partial}{\partial x}(A\alpha_m \rho_m V_m^2) =$$

$$-\alpha_m \frac{\partial p}{\partial x} + K_{mw}(V_w - V_m) - \Gamma_f V_m \tag{5}$$

and

$$\frac{\partial}{\partial t}(\alpha_f \rho_m V_f) + \frac{1}{A}\frac{\partial}{\partial x}(A\alpha_f \rho_m V_f^2) =$$

$$-\alpha_f \frac{\partial p}{\partial x} + K_{fw}(V_w - V_f) + \Gamma_f V_m. \tag{6}$$

The terms on the RHS of equations (4), (5) and (6) represent the effect of the pressure gradient force, drag between the various species (the fragments and the melt droplets are assumed to be surrounded by water so that they do not interact, i.e. $K_{fm} \equiv 0$), and momentum transfer due to mass transfer. The fragments are assumed to be moving with the melt droplet velocity at the instant they are formed. Real viscous forces have been ignored, since they are always negligible in situations of interest to us. However, one of the new features of this model is the inclusion of the artificial viscosity term in the water species momentum equation.

There are also energy conservation equations for each species. It is convenient to work in terms of the stagnation energy, defined by $e_s = e + 1/2V^2$ and the stagnation enthalpy defined by $h_s = e_s + p/\rho$. Conservation of energy for the water, melt and fragments gives:

$$\frac{\partial}{\partial t}(\alpha_w \rho_w e_{sw}) + \frac{1}{A}\frac{\partial}{\partial x}\left(A\alpha_w V_w \left(\rho_w h_{sw} - \mu_a \frac{\partial V_w}{\partial x}\right)\right)$$

$$= -p\frac{\partial \alpha_w}{\partial t} + R_{mw}(T_m - T_w) + R_{fw}(T_f - T_w)$$

$$+V_w K_{mw}(V_m - V_w) + K_{mw}(V_w - V_m)^2$$

$$+V_w K_{fw}(V_f - V_w) + K_{fw}(V_w - V_f)^2, \tag{7}$$

$$\frac{\partial}{\partial t}(\alpha_m \rho_m e_{sm}) + \frac{1}{A}\frac{\partial}{\partial x}(A\alpha_m \rho_m V_m h_{sm})$$

$$= -p\frac{\partial \alpha_m}{\partial t} + R_{mw}(T_w - T_m) + V_m K_{mw}(V_w - V_m) - \Gamma_f h_{sm} \tag{8}$$

and

$$\frac{\partial}{\partial t}(\alpha_f \rho_m e_{sf}) + \frac{1}{A}\frac{\partial}{\partial x}(A\alpha_f \rho_m V_f h_{sf})$$

$$= -p\frac{\partial \alpha_f}{\partial t} + R_{fw}(T_w - T_f) + V_f K_{fw}(V_w - V_f) + \Gamma_f h_{sm}. \tag{9}$$

In the above equations the terms involving R_{mw} etc. represent thermal equilibration and the terms containing K_{mw} etc. are the drag work. It has been assumed that all of the irreversible drag work heats up the water. For completeness, the viscous work due to the artificial viscosity term is included in the water energy equation, but this is found to be insignificant in practice.

There is also an equation for the length-scale of the melt droplets, which is given by

$$\frac{\partial}{\partial t}(\alpha_m \rho_m L_m) + \frac{1}{A}\frac{\partial}{\partial x}(A\alpha_m \rho_m V_m L_m) = -\Gamma_f L_m - \Gamma_{frag}. \tag{10}$$

In the above equation the term involving Γ_f is due to mass transfer (it is a consequence of writing the transport equation in conservation form) and the term $-\Gamma_{frag}$ models the chosen fragmentation process.

In addition to the above equations there is the constraint that

$$\alpha_m + \alpha_f + \alpha_w = 1. \tag{11}$$

This completes the specification of the differential equations. The next subsections contain a description of the constitutive relations used to close the model, the Equations of State (EOS), the form of the artificial viscosity term used, and the boundary and initial conditions.

2.2 Constitutive Relations

In this section the constitutive relations for drag, heat transfer and fragmentation employed in the model are described.

2.2.1 Momentum Exchange

If the volume fraction of droplets is α_m, there are $6\alpha_m/\pi L_m^3$ spherical droplets per unit volume. The drag force on a single droplet may be written as

$$F_D = \frac{1}{2}c_{d,mw}\rho_e \pi \frac{L_m^2}{4}|V_w - V_m|(V_w - V_m) \tag{12}$$

where $\rho_e = (\alpha_w \rho_w + \alpha_f \rho_f)/(\alpha_w + \alpha_f)$ is the effective density of the fluid dragging the melt drops. The effective density is used because there is assumed to be no direct interaction between the fragments and the unfragmented drops; the presence of the

fragments is assumed to increase the inertia of the fluid surrounding the drops. Thus the total drag force is

$$F_T = \frac{3}{4}\frac{c_{d,mw}}{L_m}\rho_e \alpha_m |V_w - V_m|(V_w - V_m) \tag{13}$$

and comparison of equation (13) with equation (5) shows that

$$K_{mw} = \frac{3}{4} c_{d,mw} \alpha_m \frac{\rho_e}{L_m} |V_w - V_m|. \tag{14}$$

In the present work a constant value of $c_{d,mw} = 2.5$ has been used. This value is higher than the usual value of 0.4 to account for the increased drag when drops are fragmenting [12].

Similarly, the drag between the melt fragments and the water is given by

$$K_{fw} = \frac{3}{4} c_{d,fw} \alpha_f \frac{\rho_w}{L_f} |V_w - V_f|, \tag{15}$$

where $c_{d,fw} = 0.4$. (The present model can be used to simulate the situation of no slip between the water and fragments by setting $c_{d,fw}$ to a large value.)

2.2.2 Heat Transfer

If the heat transfer rate is specified as the product of a heat transfer coefficient and the temperature difference, it is easily shown that

$$R_{mw} = 6\alpha_m \frac{h_{mw}}{L_m} \tag{16}$$

and

$$R_{fw} = 6\alpha_f \frac{h_{fw}}{L_f} \tag{17}$$

where h_{mw} is the heat transfer coefficient between the melt and water, h_{fw} is the heat transfer coefficient between the fragments and water and L_f is the fragment size.

The heat transfer mechanisms between the melt and water are very complex and clearly depend on the time-history of each particle. The only experimental data available is rather crude and consists of time-averaged heat transfer coefficients for the duration of the fragmentation process [9]. Thus in the present model constant values for the heat transfer coefficients have been used. A value of $h_{mw} = 10^3$ $\mathrm{Wm^{-2}K^{-1}}$ was used for the melt when it was surrounded by a vapour film. This is a typical value obtained from a combination of radiation and film boiling [9]. This value was increased by typically two orders of magnitude when vapour film collapse was judged to have occurred. This increase is somewhat less than that used in an earlier version of CULDESAC [1], since it is thought to be closer to expected values than the upper bound value used in the earlier work. However, there is considerable uncertainty as to what values actually occur in real explosions. (The effect of varying this parameter is examined in section 4.3.)

The treatment of vapour film collapse used here is simply to increase the heat transfer coefficient when the pressure exceeds a certain value, since this models pressure

induced vapour film collapse. Because of the high initial temperature of the melt ($\sim$ 3000K) in situations of interest to us, temperature controlled vapour film collapse was not considered to be important [16]. Scoping calculations show that the model predictions are insensitive to the choice of vapour film collapse pressure and melt droplet to water heat transfer coefficient, provided that reasonable values are chosen [11].

The fragment size L_f is not determined by the fragmentation model currently employed (see section 2.2.3) and was specified by reference to experimental data. A typical value of $L_f = 100\mu$m was used [14].

2.2.3 Fragmentation Model

A boundary layer stripping model for fragmentation is used, as this is thought to be the most appropriate for the study of vapour explosions [15]. The model proposed by Carachalios *et al* [15] is used. This gives the following stripping rate from a single fragment

$$\frac{\mathrm{d}m}{\mathrm{d}t} = c_{frag}|V_m - V_w|\pi L_m^2\sqrt{\rho_m\rho_e}, \tag{18}$$

where the empirical constant c_{frag} takes a value of approximately 1/6. Multiplying equation (18) by the number of drops per unit volume and comparing the result with equation (2) gives

$$\Gamma_f = \alpha_m c_{frag}|V_m - V_w|\sqrt{\rho_e\rho_m}/L_m \tag{19}$$

where all of the constant terms have now been included in c_{frag}, so that $c_{frag} \sim 1$. Thus the mass stripping rate is proportional to the relative velocity and the square root of the effective density. As fragmentation occurs, the density of the surrounding fluid is increased by the addition of fragments and thus the fluid has more inertia to fragment the drops further.

The length-scale of the droplets is changed by the mass loss due to boundary layer stripping. For spherical drops it is easily shown that the mass loss rate given in equation (19) implies a length-scale source term of

$$\Gamma_{frag} = \frac{1}{3}\Gamma_f L_m \tag{20}$$

which is not surprising, as equation (20) implies that a droplet's length-scale changes at one third the rate of its volume. An empirical function has been added to ensure that breakup only occurs for Weber numbers above a critical value ($\mathrm{We}_{crit} \approx 12$). Details are given elsewhere [17].

2.3 Equations of State

The melt equation of state is very simple. The melt is assumed to be incompressible so that $\rho_m = \rho_f =$ constant, and to have a simple caloric equation of state so that $E_m = c_{vm}T_m$ and $E_f = c_{vm}T_f$.

The EOS for water is more complicated and there is virtually no thermodynamic data on the properties of water at high temperatures and pressures in a suitable form for use in a model such as this one. In this study an approximate EOS, based on the Grüneisen approximation, has been used. The equation of state is fully described in

reference [1] and has been shown to agree well with steam table data in the region where they can be compared [10].

2.4 Artificial Viscosity

In an earlier version of the CULDESAC code [1, 10] the conservation equations were solved without the inclusion of an artificial viscosity term. This procedure was found to work well, provided that the water density behind the front was not too great. For example, a series of calculations performed to examine the effect of varying the void fraction (the fraction of the water phase in vapour form) ahead of the front, showed the increased presence of high frequency oscillations in the pressure at the front with falling void fraction [1]. Simulations also showed that decreasing the heat transfer rate from the fragments to the water led to these oscillations [10]. In some cases a solution could not be obtained beyond a certain time because these oscillations caused unphysical compression of the water (they led to densities outside the liquid region of the phase plane).

In this version of the model an artificial viscosity term is included in the water species momentum equation in order to remove this instability. The chosen form is that advocated by von Neumann and Richtmyer [18] and discussed by Richtmyer and Morton [19]. The artificial viscosity, μ_a, is assumed to be of the following form:

$$\begin{aligned} \mu_a &= \rho_w (b_0 \Delta x)^2 \left| \frac{\partial V_w}{\partial x} \right| \qquad \text{if } \frac{\partial V_w}{\partial x} < 0, \\ &= 0 \qquad \text{otherwise.} \end{aligned} \tag{21}$$

This form for μ_a has the property that viscosity is only added in regions of flow compression, i.e. it does not smear out expansion fans and it is only added where there are large velocity gradients, i.e. at the shock front itself. It is consistent with the original differential equation in that $\mu_a \rightarrow 0$ as $\Delta x \rightarrow 0$. However, as discussed elsewhere [20], it is not sensible to insist on the requirement that the solution should converge as $\Delta x \rightarrow 0$, since the original equations do not contain, for example, viscous terms.

In the original work of von Neumann and Richtmyer, it was shown that if the constant b_0 was chosen to be of order unity, then the shock would be spread over approximately three grid cells. This conclusion was based on analysis for an *ideal gas* equation of state. In this application values of b_0 of order 5–15 were used, with higher values required for the less compressible initial condition, i.e. for low initial void fractions or low heat input rates. Higher values of b_0 are required because the equation of state of water is much 'stiffer' than that of an ideal gas.

2.5 Boundary and Initial Conditions

The above equations are solved in a solution domain which represents an initial mixture contained in a closed vessel. Thus the only boundary condition needed is to set the velocities to zero at the vessel walls.

Initially, the volume fractions, void fraction, velocity and particle size distribution are specified. To simulate triggering a fraction of the melt is fragmented in a small region of the solution domain. This causes a high heat transfer rate in these cells, the pressure rises locally and a detonation wave may develop.

3 Solution Procedure

The partial differential equations are solved using a finite difference method which employs the usual staggered grid arrangement. All convective terms are modelled using upwind differencing for stability. An implicit scheme is used, with all physical terms, except for the rates obtained from constitutive laws, being evaluated using mid-time values. (Mid-time values are obtained by taking the average of the old time value and the new time-value obtained from the previous iteration step.) The fragmentation, heat transfer and drag rates are evaluated using old time values, once and for all, at the beginning of each time-step. The artificial viscosity term in the water momentum equation is treated fully implicitly for stability. The same basic strategy as described in references [1, 21] is employed, except that iteration must now be carried out at each time-step. Superscripts n and $n+1$ are used to denote old and new time values respectively. At any time during the calculation new time values of the field variables are obtained using the following procedure:

1. determine the fragmentation, heat transfer and drag rates using old time values;

2. equations (1) $\rightarrow$ (3) are used to obtain $(\alpha_w \rho_w)^{n+1}$, α_m^{n+1} and α_f^{n+1}, respectively. Equation (11) is then used to determine α_w^{n+1} and hence ρ_w^{n+1} can be determined;

3. equations (4) $\rightarrow$ (6) are used to obtain the new velocity fields. A tri-diagonal matrix is solved for each species, with the momentum flux, pressure gradient and drag terms evaluated using the latest estimates of the mid-time values;

4. the new stagnation energies are found by time advancing the three energy equations (7) $\rightarrow$ (9). Using the stagnation form ensures that the Rankine-Hugoniot equation can be built into the solution scheme to give it good shock-capturing properties. The new velocity field is then used to determine the new internal energies;

5. the caloric equations are used to determine the new melt and fragment temperature. The water EOS is then used to determine the new pressure field and the water temperature;

6. a check is made to determine the largest change in the pressure, in each cell, from that calculated at the previous iteration step, normalised by the pressure in that cell. If this is less than 10^{-3}, equation (10) is solved to obtain the new melt length-scale and the iteration cycle is finished. If it is not, new mid-time values are calculated using the latest estimate of the values at the time level $n+1$ and the iteration process starts again at step 2.

This completes a brief description of the numerical scheme, which has proved to be very robust and stable. Typically three iterations are required at each time-step. Because an implicit method is being used, the time-step can exceed the value used in the previous version of the code by about two orders of magnitude. The main restriction on the time-step is that imposed by the need to model rate processes, such as fragmentation, accurately.

Parameter	Value	unit
Time-step	10^{-6}	s
Space-step	0.005	m
Coefficient in artificial viscosity term (b_0)	15.0	—
Initial particle size	0.005	m
Initial pressure	0.1	MPa
Heat transfer rate: vapour blanketed	10^3	$Wm^{-2}K^{-1}$
Heat transfer rate: liquid-liquid contact	10^5	$Wm^{-2}K^{-1}$
Pressure required to collapse vapour blanket	1.0	MPa
Initial melt temperature	3400	K
Melt density	8400	kgm^{-3}
Melt heat capacity	500	$Jkg^{-1}K^{-1}$
Melt surface tension	0.4	Nm^{-1}
Initial melt volume fraction	0.1	—
Initial void fraction	0.5	—
Length of triggered zone	0.02	m
Fraction of melt fragmented as a trigger	0.9	—

Table 1: Parameters used in the detonation simulations

4 Example Simulations

The next three subsections contain results obtained for the case when the fragments are assumed to move with the water species, i.e. obtained using a large value of $c_{d,fw}$. These results are then for the *same* physical model as used in previous simulations [1]. In the first subsection the properties of the solution scheme are studied. The next two subsections contain results obtained from a computational study of the effect of varying the initial void fraction and the heat transfer rate between the fragments and the water. Some results obtained from a study where the fragments are not assumed to move with the water velocity are presented in section 4.4. Unless otherwise stated the conditions shown in table 1 are used in the calculations. All of the simulations are for a planar geometry, i.e. $A \equiv 1$.

Figure 2 shows the results from a simulation of the development of the pressure profile as a function of time for the conditions given in table 1. (Profiles are shown every 0.5ms.) Also shown, as a dotted line, is the development of the pressure profile for the case where no artificial viscosity was added. This latter calculation fails after 1.5ms because unphysical density values are produced (the liquid density exceeds values obtainable for liquid water). This comparison shows that the instability at the front has been cured.

4.1 Properties of the Numerical Scheme

As with all numerical work, it is important to understand the effect of solution parameters on the results obtained from the finite difference scheme. There are essentially four parameters to consider: (i) the time-step Δt; (ii) the space-step Δx; (iii) the artificial viscosity coefficient b_0; and, (iv) the convergence criterion used to terminate the iteration scheme.

By reducing the time-step and the convergence criterion it was found that the solution was independent of these parameters for the values chosen. In fact the time-step can be increased so that the Courant number exceeds unity without any problem. This is because the scheme is fully implicit. However, the Courant numbers was $\sim$0.4 in most calculations, since the time-step is limited by the requirement that rate processes be properly resolved.

The results of a space-step refinement study are shown in figure 3. In this calculation the initial void fraction was 0.1 and the artificial viscosity coefficient was set to 15. The figure shows the pressure profile for three different cases, $\Delta x = 2.5, 5$ and 10mm, 2.5ms after triggering. The same trigger was used in each simulation. (The time-step was also changed so that the Courant number is the same in each simulation.) It is evident from the figure that the solution obtained with a 5mm grid is not significantly different from that obtained from a 2.5mm grid. In fact the average velocity of the front varies from 360ms^{-1} for the 10mm grid to 380ms^{-1} for the 2.5mm grid, which would be well within experimental error if such data were available. Further grid refinement is not sensible, since the validity of the inviscid multiphase flow equations is questionable even at this level of grid refinement [20]. Thus it was decided to use a 5mm grid in all future calculations.

The effect of varying the artificial viscosity coefficient was examined for a case where a solution could be obtained with zero artificial viscosity. In order to do this an initial void fraction of 0.7 was chosen. Figure 4 shows the pressure profile 2.5ms after triggering for values of b_0 of 0, 6, 8 and 10. It is evident that there is not a significant difference between the results obtained with the non-zero values of b_0. Increasing b_0 increases the shock speed but not significantly. The instability at the front, which is significant when there is no artificial viscosity, is fully removed when b_0 is set to a value of 8. Thus it may be concluded that the choice of b_0 does not affect the solution to within experimental accuracy, provided a reasonable choice is made. Experience of using the model shows when too small or too large a value of b_0 has been used.

4.2 The Effect of Initial Void Fraction

It is apparent from the results already presented that the initial void fraction of the mixture can affect the shape of the pressure profile and the speed of the detonation front. This section contains a detailed study of this effect. It is important to know how the initial void fraction affects the detonation behaviour because it is one of the principal unknowns in the data used to validate this type of model [9] and it varies considerably with melt temperature. For example, experiments using molten aluminium at say 1000K poured into water lead to very different premixtures from molten uranium dioxide at 3400K poured into water. In the first case high volume fractions of liquid water can exist within the mixture, whereas at the higher melt temperature the liquid

fraction is very low [22].

Figure 5 shows the predicted pressure profile 2ms after triggering for a range of initial void fractions. It is evident that decreasing the initial void fraction leads to flatter pressure profiles, with the heat being input over a much longer spatial distance. This is because the fragmentation process is less efficient when the pressure at the shock front is lower. The very flat pressure profiles predicted for low initial void fractions are similar in shape to those predicted for tin-water detonations by Sharon and Bankoff [23]. In the case of tin and water there is very little thermal energy in the tin and so the water is not heated significantly if the heat is added to all of the water present [9].

It is also apparent from the figure that the speed of the detonation front varies considerably with initial void fraction. Figure 6a shows the *average* speed of the front over the first 2ms of the calculation. It is evident that the speed has a minimum value for a void fraction of $\sim$0.3. Figure 6b shows the experimental data of Miyazaki *et al* [24] for the speed of pressure waves in air-water mixtures. The figure shows that the present model predicts similar behaviour for detonation waves. The minimum speed occurs at about the same void fraction in the two different cases. Also, the increase in the speed away from this minimum is seen to be much faster in the low void fraction region than in the high void fraction region, a feature which is, again, a prediction of the present model. The speeds are very different in the two cases because of the heat energy addition in the detonation case.

It is also of interest to examine the detailed variation of properties, such as the volume fractions, water density, velocities and temperatures across the interaction zone. Simulations were performed for three different void fractions, namely 0.1, 0.3 and 0.9, these corresponding to the two ends and minimum point on the plot of detonation velocity against void fraction (see figure 6a). The calculations were terminated when the detonation front had travelled approximately 0.9m, this corresponded to times since triggering of 2, 3 and 2.5ms, respectively.

Figures 7a–c show the three volume fractions for the three cases described above. At the lowest void fraction it is evident that complete fragmentation of the melt does not occur. At a void fraction of 0.3 the fragmentation zone is $\sim$0.5m long and for a void fraction of 0.9 the zone is 0.15m long. This is because a much stronger detonation develops for high initial void fractions with the present modelling assumptions. The behaviour of the fragments is also very different in the three cases. At low initial void fractions the particles remain where they are formed but for a high initial void fraction they tend to follow the detonation front, increasing the compression at the front. In the calculations presented here the particles are assumed to move with the water species; the effect of allowing for a finite drag rate is considered later.

The water density for the three different cases is shown in figures 8a–c. It is clear that at low initial voids fractions there is far greater compression of the water at the detonation front but that the density falls rapidly behind the front. The effect of allowing for this density difference on the heat transfer rate is considered in part II of this paper. In all cases there is an anomalous region close to the wall at which triggering was assumed to occur, however, this behaviour is confined to the first 0.1m of the solution domain.

Figures 9a–c show the velocity fields for the three different cases. Again it is evident that there is very different behaviour in the three cases. At high initial void fractions

the shock front is very steep and very strong. At low initial void fractions there is some smearing of the shock front but the main feature is the much reduced fluid velocity and the much longer flow zone in the low void fraction case.

Finally, figures 10a–c show the predicted temperature fields for the three different cases. Heat transfer is seen to be more rapid at high void fraction but in all cases the heat transfer zone is very long and heat transfer is far from complete in the low initial void fraction cases. Thus a large system dimension would be required for a steady-state detonation to develop.

4.3 The Effect of Varying the Heat Transfer Rate

The heat transfer rate from the fragments to the water is a very important parameter in the model. However, this quantity is not well-known because of the experimental difficulties of measuring the transient heat transfer rate under these sort of conditions, i.e. millisecond timescales and high temperatures and pressures. A recent review of the available data [9] concluded that heat transfer coefficients in the range 10^5–$10^6\,\mathrm{Wm^{-2}K^{-1}}$ are appropriate when heat transfer is to a high density fluid. The lower value corresponds to liquid-liquid conduction and the higher value corresponds to enhanced boiling.

Figures 11 and 12 show the development of the pressure field with time for heat transfer coefficients of $10^5\,\mathrm{Wm^{-2}K^{-1}}$ and $10^6\,\mathrm{Wm^{-2}K^{-1}}$, respectively. The initial void fraction was 0.5 and pressure traces are shown every 0.2ms. There is a considerable difference between the two figures, showing the importance of knowing the heat transfer rate. At the lower value of h_{fw} the pressure profiles show no evidence of a von Neumann spike and are apparently far from reaching a steady-state even after a distance of 0.9m has been travelled. At the higher heat transfer rate there is a well-developed von Neumann spike and the pressure profile is much closer to reaching a steady-state. Also the average velocity in the high heat transfer rate case is approximately double that in the low heat transfer rate case. Thus although the model predictions are very sensitive to the heat transfer rate, it should be possible to design experiments to determine which value of the heat transfer rate produces pressure profiles the closest to those observed experimentally.

Comparison of the shapes of the pressure profiles shown in figures 11 and 12 with those shown in figure 5 leads one to the conclusion that reducing the heat transfer rate is in some sense equivalent to reducing the initial void fraction. This is easy to explain. If the heat transfer rate is high or the initial void fraction is high (recall that in these simulations the heat transfer rate does not depend on the flow regime), then supercritical conditions are reached a short distance behind the shock front and the pressure rise is high. However, if the heat input rate is low or the initial void fraction is low then the water phase is heated up more slowly and no pressure spike is formed.

4.4 The Effect of Allowing Slip Between the Water and Fragment Phases

The effect of relaxing the assumption that the fragments and the water move with the same velocity is examined briefly in this section. The case of a void fraction of 0.9 and a heat transfer coefficient of $10^5\mathrm{Wm^{-2}K^{-1}}$ is considered. This is a case, shown in

figures 7–10, where there is a significant accumulation of particles behind the detonation front. (All other conditions, except for b_0=10, are the same as those shown in table 1.) Figure 13 shows a comparison of the pressure profiles obtained 2ms after triggering for cases where $c_{d,fw} = 0.4$ and 75, the latter value giving fragment and water velocity which were identical almost everywhere. It is clear from the figure that the two solutions are not very different, apart from the fact that the sharp spike present in the no-slip case is 'rounded' in the case where slip is allowed. The shock speed and steady-state pressurization behind the front are almost identical.

Figure 14 shows a comparison of the velocity fields in the two different cases. It is apparent from figure 14a that in the case of a large drag coefficient there is virtually no slip between the fragments and the water. However, figure 14b shows that when $c_{d,fw} = 0.4$ there is considerable slip between the fragments and the water phase throughout the solution domain. (In both figures the melt velocity field in the first 0.8m is of no significance since the melt particle fraction is very small in this zone.) This slip between the water and fragments leads to some 'rounding' of the fragment void fraction profile near the shock front but the effect is not significant.

Thus it may be concluded that allowing for slip between with fragments and the water phase is not an important feature of the model once a detonation has developed. However, this may not be the case when the initial escalation stage is considered, especially if the trigger is weak.

5 Conclusions

An improved model of melt/water detonations has been described. The model uses the usual multiphase flow equations to simulate the passage of a detonation wave through a mixture of melt and water. The model assumes that differential acceleration of the melt and water, by the passage of a shock front, causes relative velocity induced fragmentation of the melt. This fragmentation, together with the collapse of the vapour blanket, leads to the development of a detonation wave. The paper describes a new solution algorithm which allows strong shocks to be captured and extends the range of applicability of an earlier model [1] considerably.

The model has been used to study the effect of the initial mixture void fraction on the propagation behaviour and to examine the effect of varying the fragment to water heat transfer rate. It is shown that a wide range of propagation velocities and pressure profile shapes are predicted using the present model. The model predicts a dependence of the detonation velocity on initial void fraction which is very similar to that observed for pressure pulses in an air-water mixture. An extension of the model to allow for slip between the fragments and water phases has been made. It is shown that this effect is not important once a detonation develops.

In part II of this paper [2] the initial escalation phase, following triggering, is studied in more detail, and the effect of varying some of the constitutive physics assumptions is examined.

Acknowledgements

This work was funded by the General Nuclear Safety Research (GNSR) Programme. They author is very pleased to acknowledge Drs. R.P. Anderson and D. Cho of Argonne National Laboratory, Dr. M. Berman of Sandia National Laboratory and Dr. A. Thyagaraja of Culham Laboratory for stimulating technical discussions on this subject.

References

[1] D.F. Fletcher and A. Thyagaraja, *A mathematical model of melt/water detonations.* Appl. Math. Modelling, **13**, 339–347, (1989).

[2] D.F. Fletcher, An improved model of melt/water detonations, part II: a study of escalation. Culham Laboratory report: CLM–P892, (1990).

[3] G. Long, *Explosions of molten metal in water—causes and prevention.* Metals progress, **71**, 107–112, (1957).

[4] D.L. Katz and C.M. Sliepcevich, *Liquefied natural gas/water explosions: cause and effect.* Hydrocarbon Process, **50**, 240–244, (1971).

[5] R.C. Reid, *Rapid phase transitions from liquid to vapor.* Advances in Chemical Engineering, **12**, 105–208, (1983).

[6] S.A. Colgate and T. Sigurgeirsson, *Dynamic mixing of water and lava.* Nature, **244**, 552–555, (1973).

[7] M.L. Corradini, B.J. Kim and M.D. Oh, *Vapour explosions in light water reactors: a review of theory and modelling.* Prog. Nucl. Energy, **22**, 1–117, (1988).

[8] S.J. Board, R.W. Hall and R.S. Hall, *Detonation of fuel coolant explosions.* Nature, **254**, 319–321, (1975).

[9] D.F. Fletcher and R.P. Anderson, *A review of pressure-induced propagation models of the vapour explosion process.* Culham Laboratory report: CLM–P879, (1990) (To appear in Progress in Nuclear Energy).

[10] D.F. Fletcher and A. Thyagaraja, *Multiphase detonation modelling using the CULDESAC code.* Paper presented at 12th Int. Col. on Dynamics of Explosions and Reactive Systems, Ann Arbor, Michigan, 23–28 July, 1989. (Also available as Culham Laboratory report: CLM–P855, (1988) and to appear in Progress in Astronautics and Aeronautics.)

[11] D.F. Fletcher, *Some computations of detonations using the CULDESAC code.* Culham Laboratory report: CLM–R291, HMSO, (1989).

[12] M. Pilch and C.A. Erdman, *Use of breakup time data and velocity history data to predict the maximum size of stable fragments for acceleration-induced breakup of a liquid drop.* Int. J. Multiphase Flow, **13**, 741–757, (1987).

[13] M. Ishii, *Thermo-fluid dynamic theory of two-phase flow.* Eyrolles, Paris, (1975).

[14] D.F. Fletcher, *The particle size distribution of solidified melt debris from molten fuel-coolant interaction experiments.* Nucl. Engng. Des., **105**, 313–319, (1988).

[15] C. Carachalios, M. Bürger and H. Unger, *A transient two-phase model to describe thermal detonations based on hydrodynamic fragmentation.* Proc. Int. Meeting on LWR severe accident evaluation, Cambridge, Massachusetts, 28 August—1 September, (1983).

[16] T.A. Dullforce, D.J. Buchanan and R.S. Peckover, *Self-triggering of small-scale fuel-coolant interactions: 1. experiments.* J. Phy. D. Appl. Phys., **9**, 1295-1303, (1976).

[17] D.F. Fletcher and A. Thyagaraja, *Multiphase flow simulations of shocks and detonations, Part III: Droplet laden gas flows.* Culham Laboratory Report: CLM–R283, HMSO, (1988).

[18] J. von Neumann and R.D. Richtmyer, *A method for the numerical calculation of hydrodynamical shocks.* J. Appl. Phys., **21**, 232–237, (1950).

[19] R.D. Richtmyer and K.W. Morton, *Difference methods for initial-value problems.* Interscience, New York, (1967).

[20] A. Thyagaraja and D.F. Fletcher, *The nonhyperbolicity of multiphase flow equations: a nonlinear nonproblem?* Comput. Phys. Commun., **56**, 115–127, (1989).

[21] D.F. Fletcher and A. Thyagaraja, *Some calculations of shocks and detonations for gas mixtures.* Comput. Fluids, **17**, 333–350, (1989).

[22] D.F. Fletcher and A. Thyagaraja, *A mathematical model of premixing.* Proc. 25th National Heat Transfer Conference, Houston, Texas, 24-27 July, 1988, ANS, HTC–**3**, 184–194, 1988.

[23] A. Sharon and S.G. Bankoff, *On the existence of steady supercritical plane thermal explosions.* Int. J. Heat Mass Transfer, **24**, 1561–1572, (1981).

[24] K. Miyazaki, Y. Fujii-e and T. Suita, *Propagation of pressure wave in air-water two-phase system (I).* Nucl. Sci. Tech., **8**, 606–613, (1971).

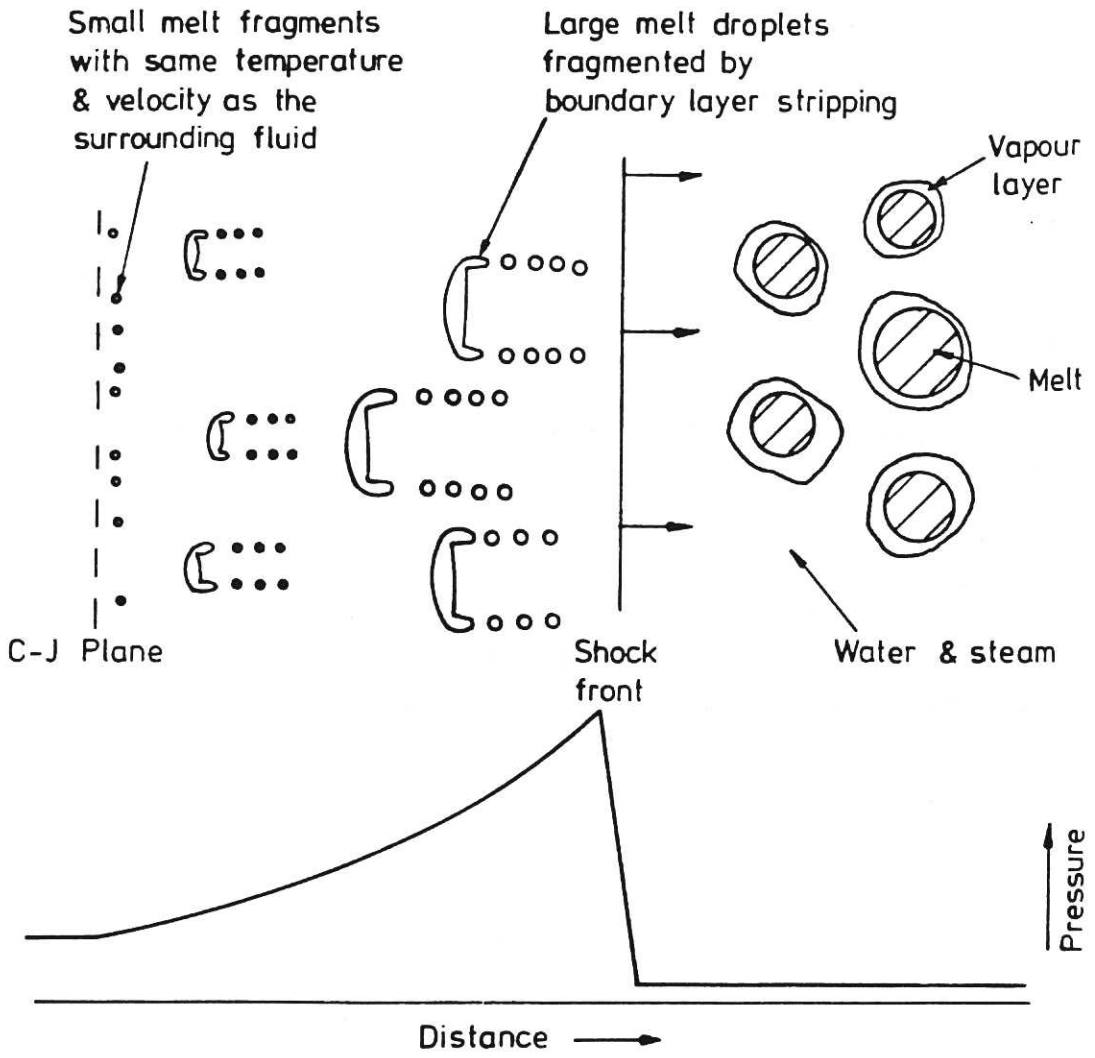

Figure 1: A schematic representation of physical picture underlying the model.

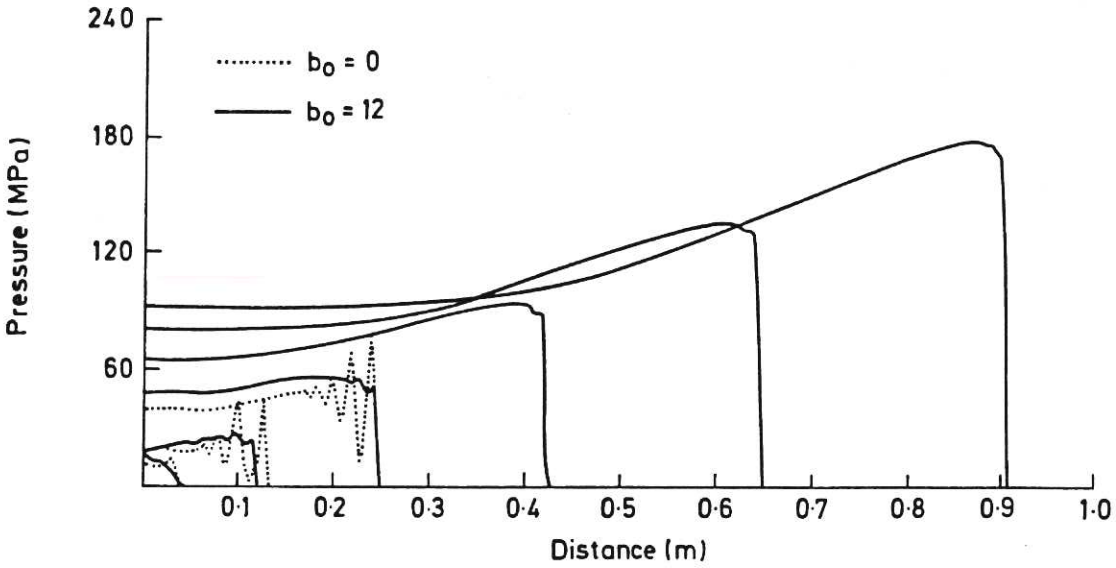

Figure 2: A comparison of the development of the pressure profile for simulations with and without artificial viscosity. The initial void fraction is 0.5 and pressure profiles are shown every 0.5ms

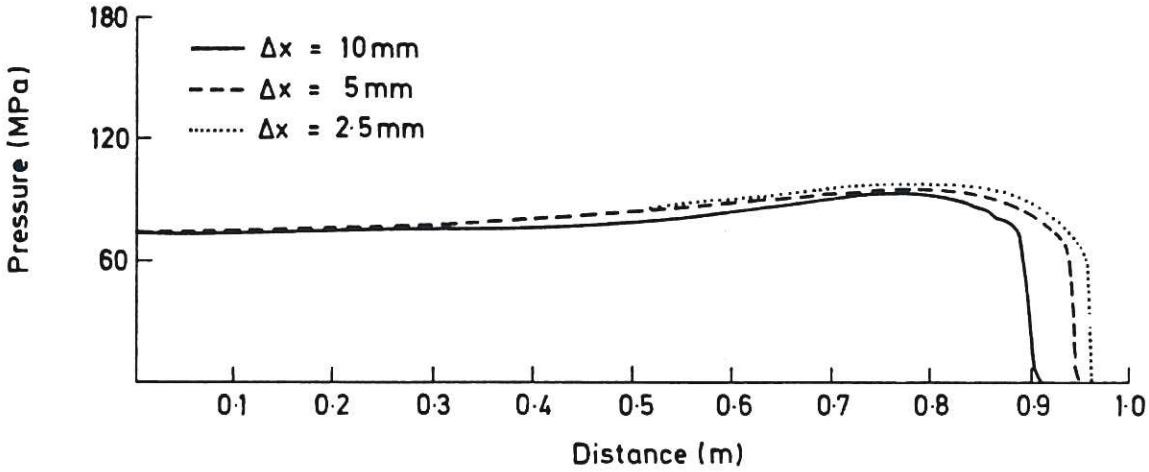

Figure 3: The effect of the choice of space grid on the predicted pressure profile.

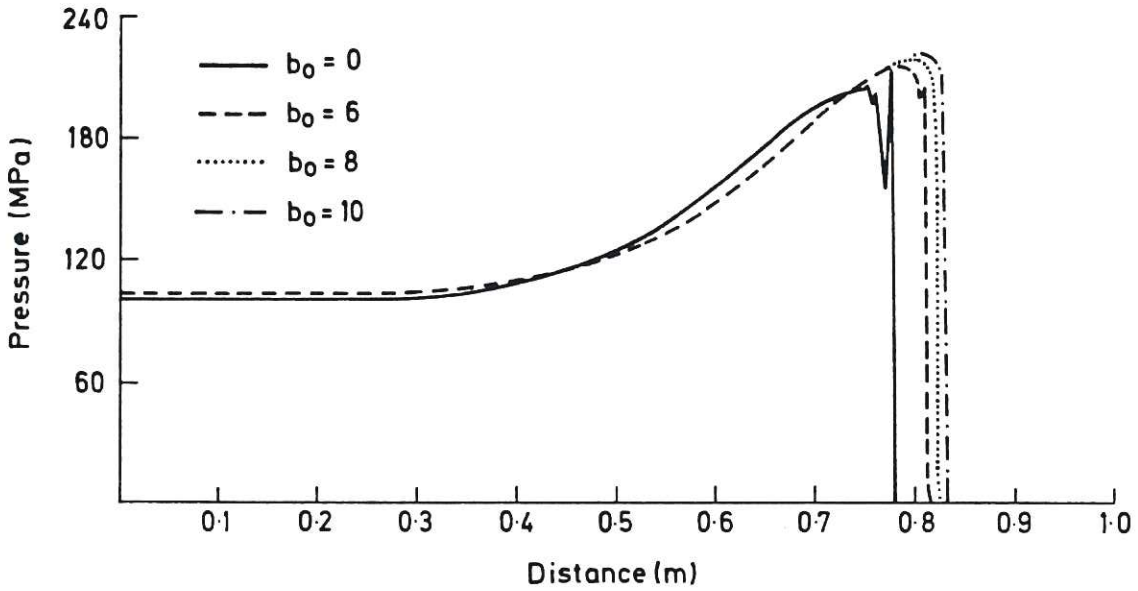

Figure 4: The results of a study of the effect of the size of the artificial viscosity coefficient on the predicted pressure profile. Note the complete removal of the instability for values of b_0 greater than 6.

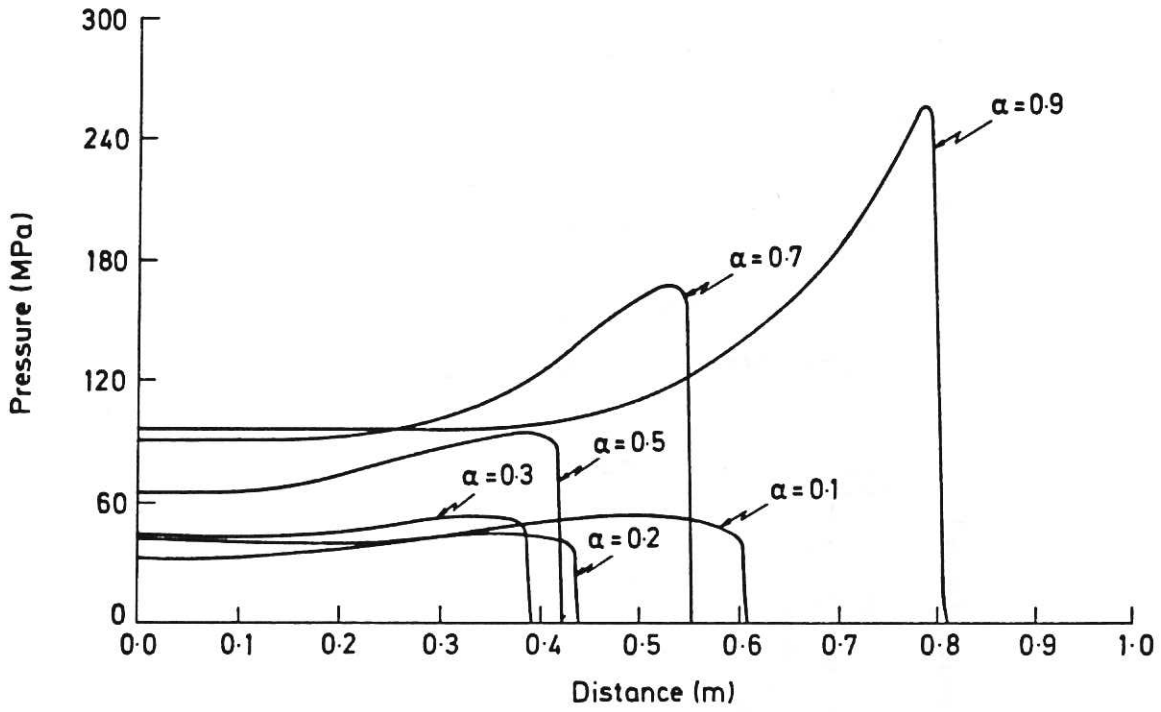

Figure 5: A comparison of the shape of the pressure profile for a range of initial void fractions.

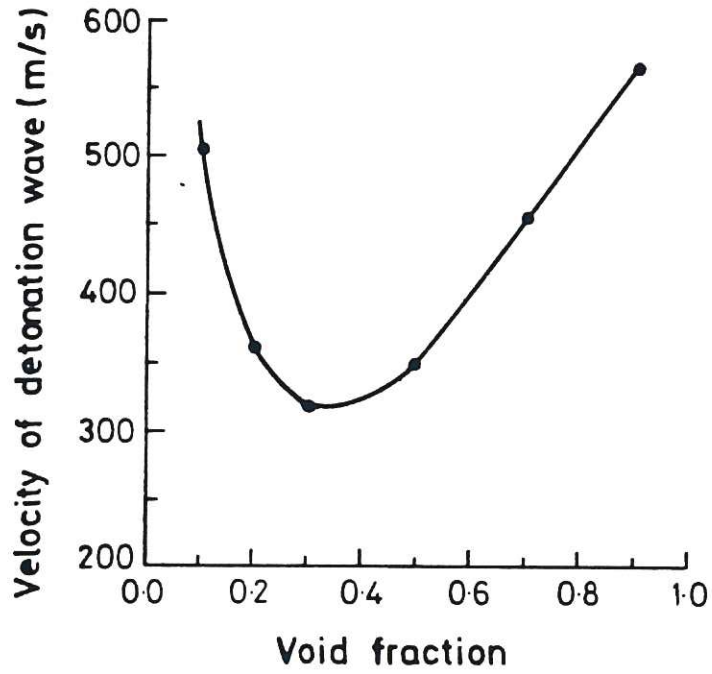

(a) Detonation wave velocity

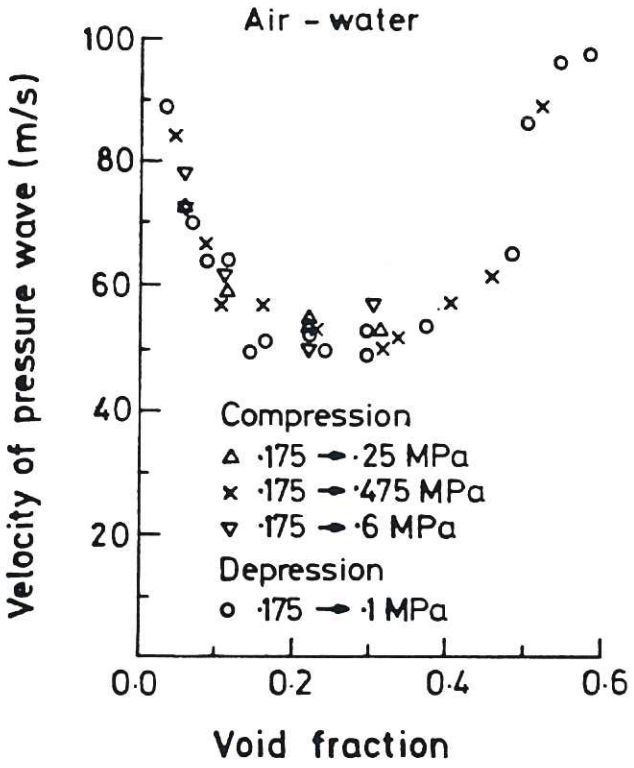

(b) Pressure wave velocity

Figure 6: The effect of initial void fraction on the shock front speed: (a) as predicted for detonations using the present model; and (b) as measured by Miyazaki *et al.* for air-water mixtures (taken from [24]).

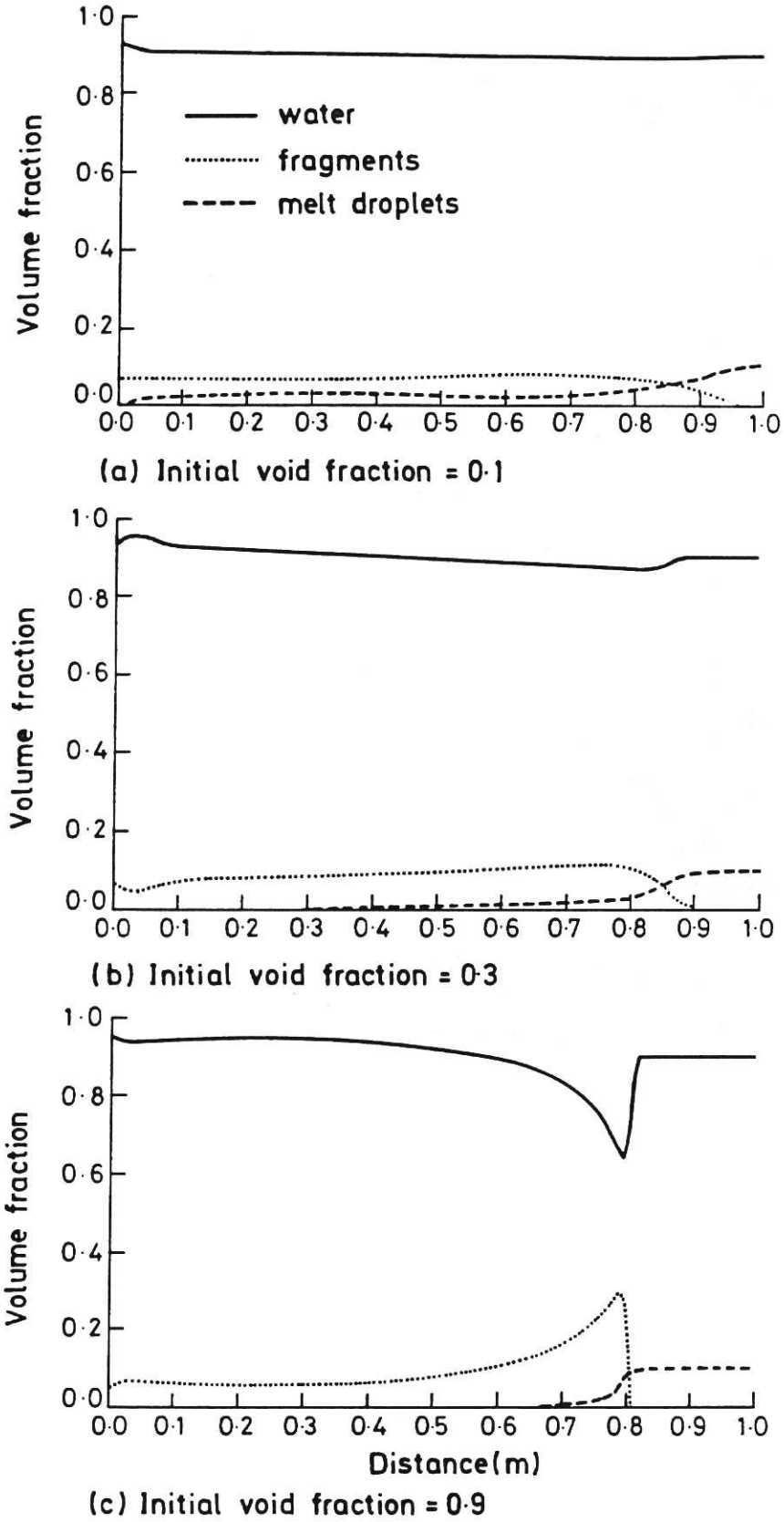

Figure 7: The volume fraction profiles for three different initial void fractions.

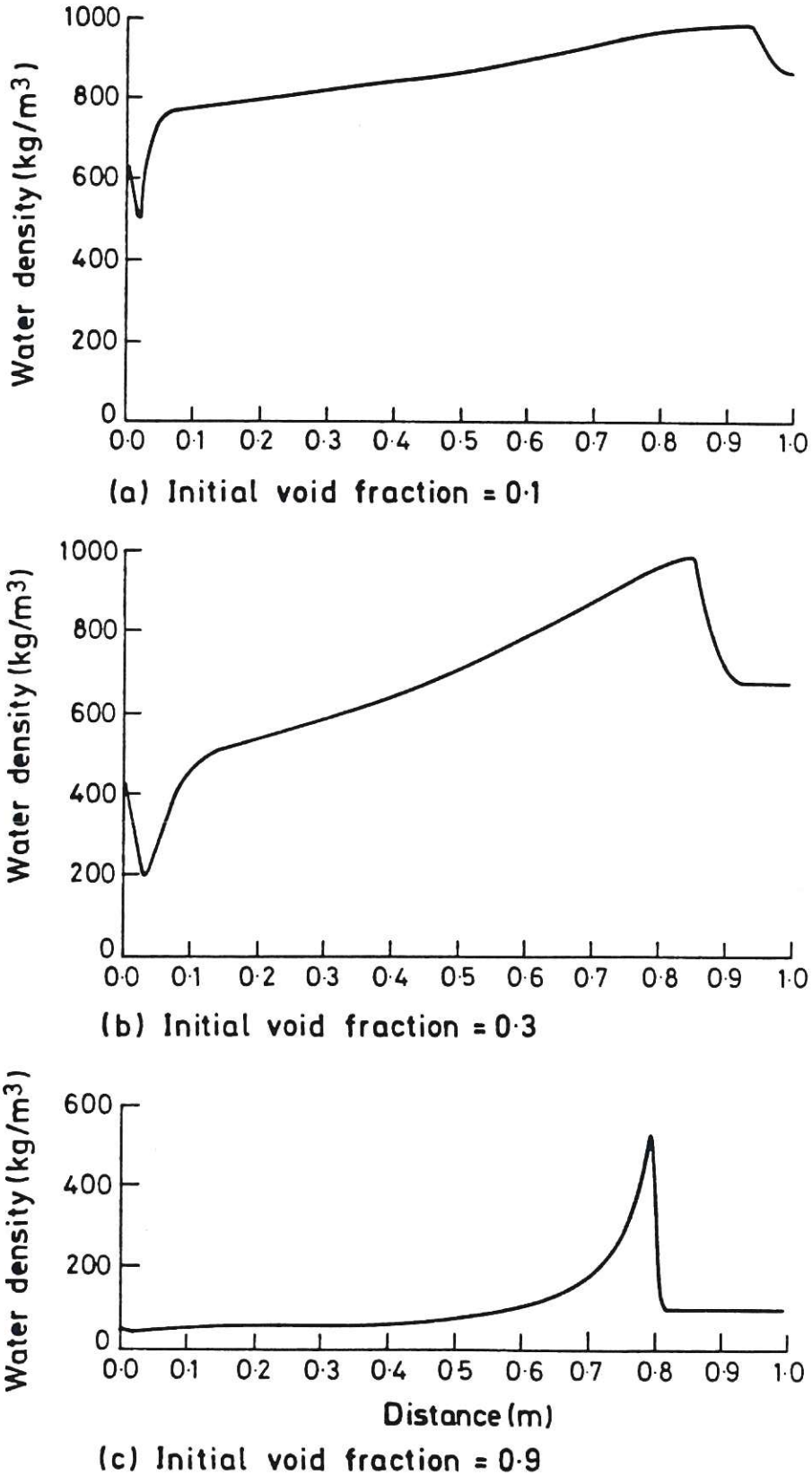

Figure 8: The water density profiles for three different initial void fractions.

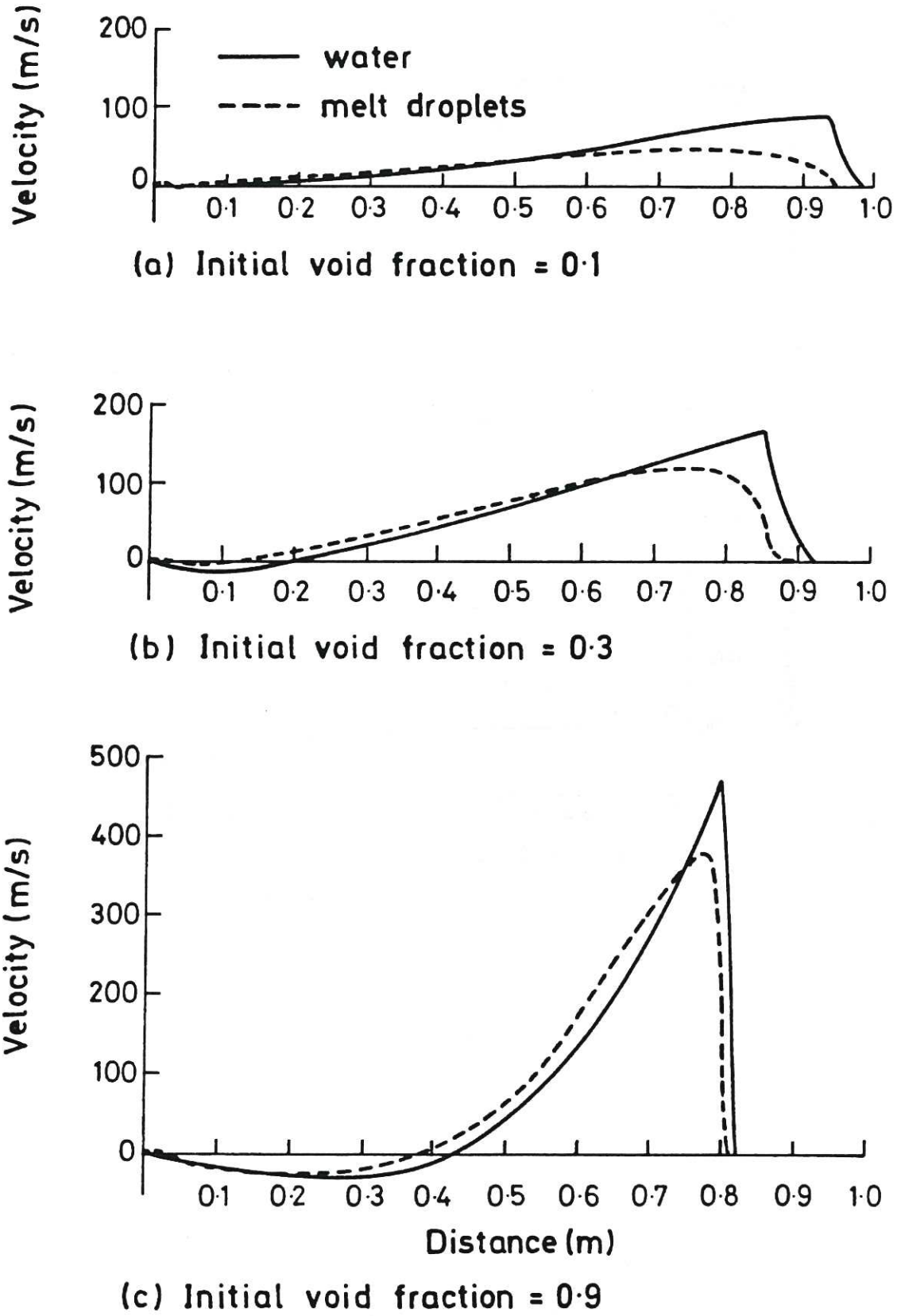

Figure 9: The velocity profiles for three different initial void fractions.

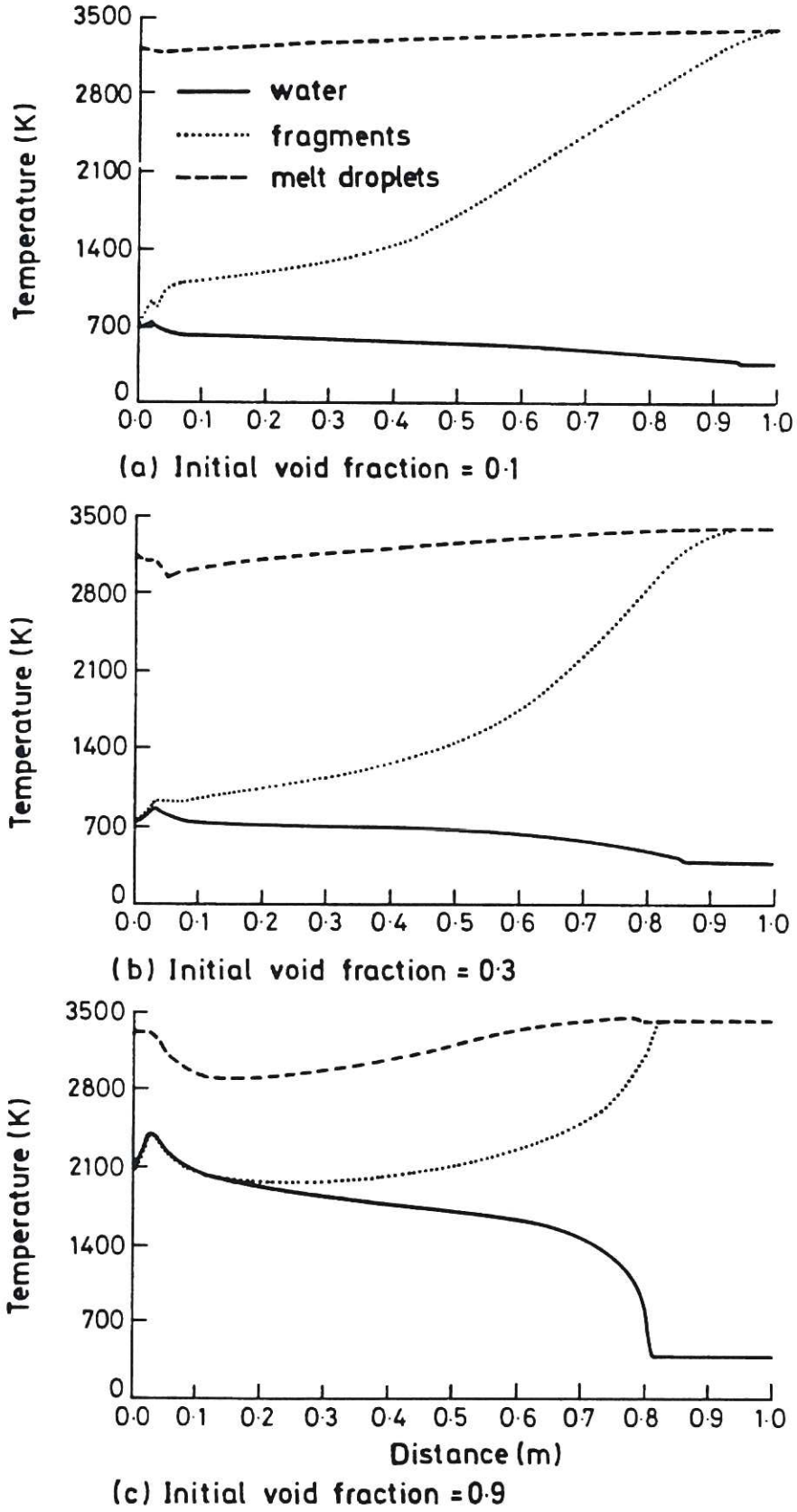

Figure 10: The temperature profiles for three different initial void fractions.

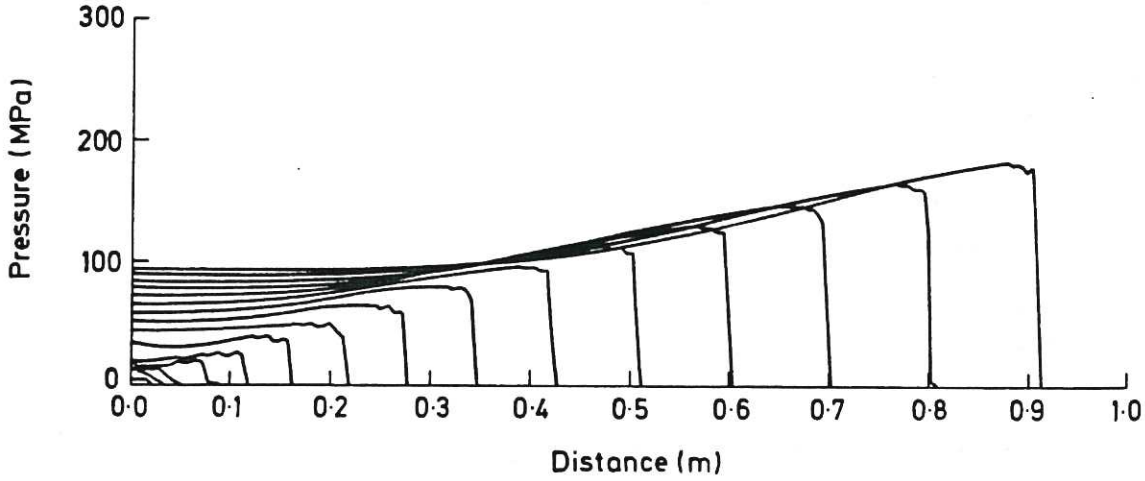

Figure 11: The development of the pressure profile for an initial void fraction of 0.5 and a fragment to water heat transfer coefficient of $10^5\,\mathrm{Wm^{-2}K^{-1}}$. (Pressure profiles are shown every 0.2ms.)

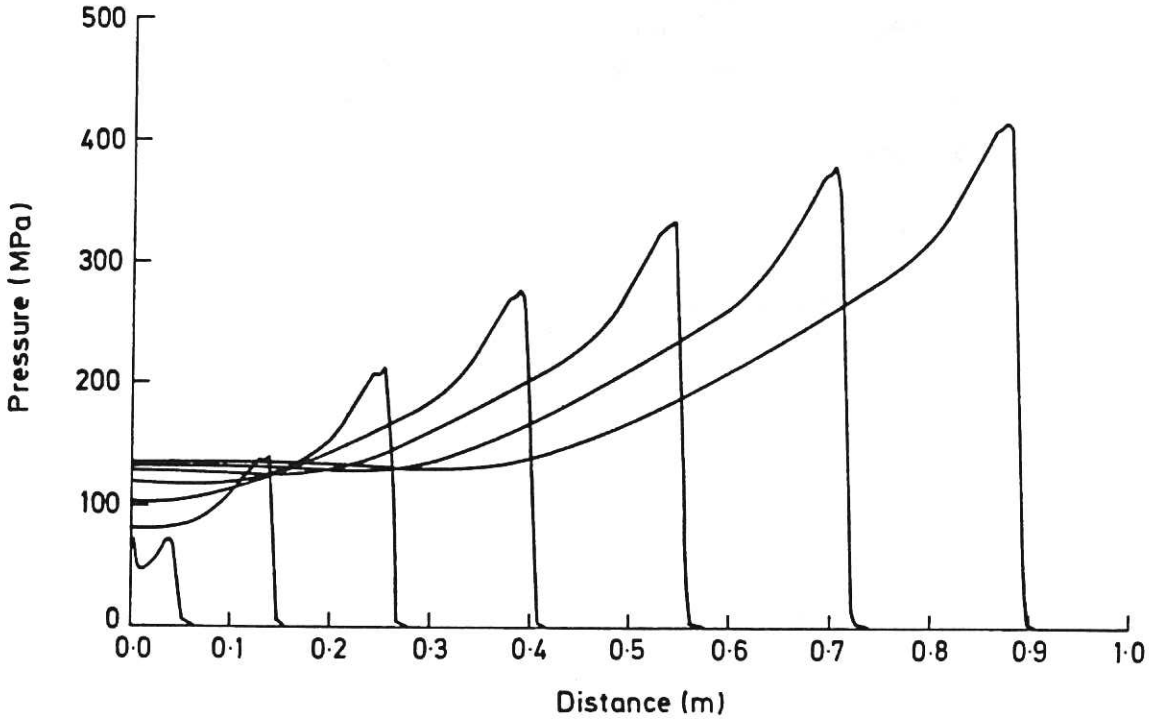

Figure 12: The development of the pressure profile for an initial void fraction of 0.5 and a fragment to water heat transfer coefficient of $10^6\,\mathrm{Wm^{-2}K^{-1}}$. (Pressure profiles are shown every 0.2ms.)

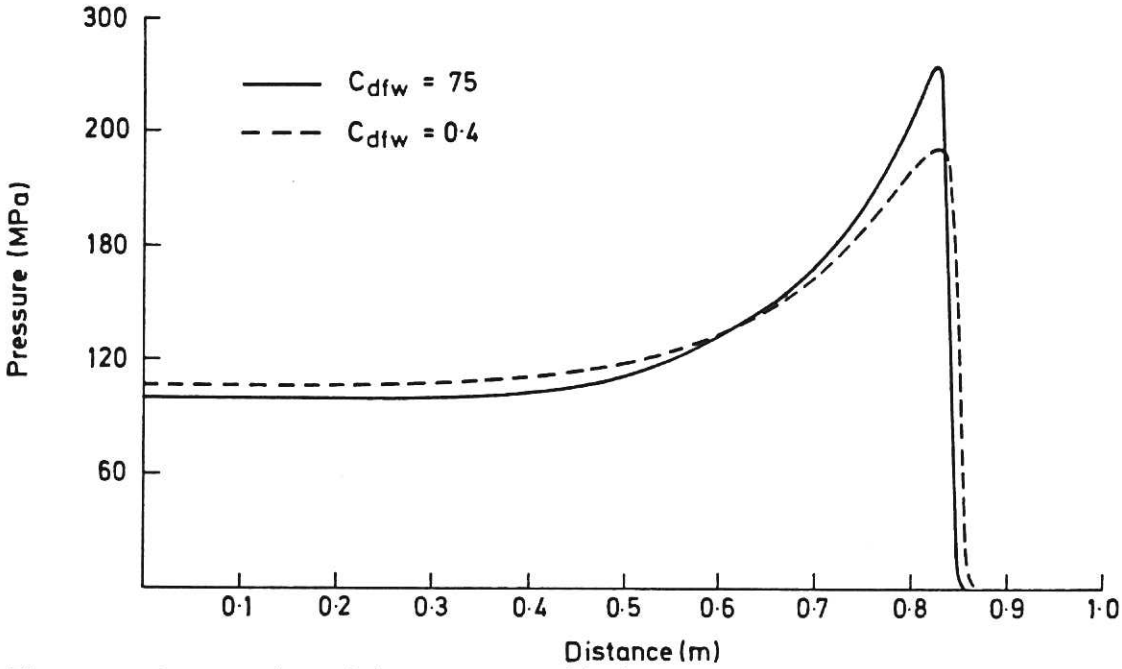

Figure 13: A comparison of the pressure profiles for cases with and without slip between the fragment and water phases. Note the rounding of the von Neumann spike in the case where slip is allowed.

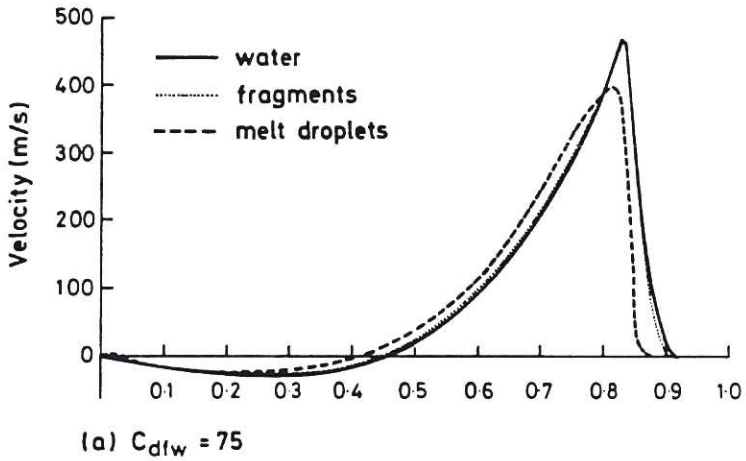

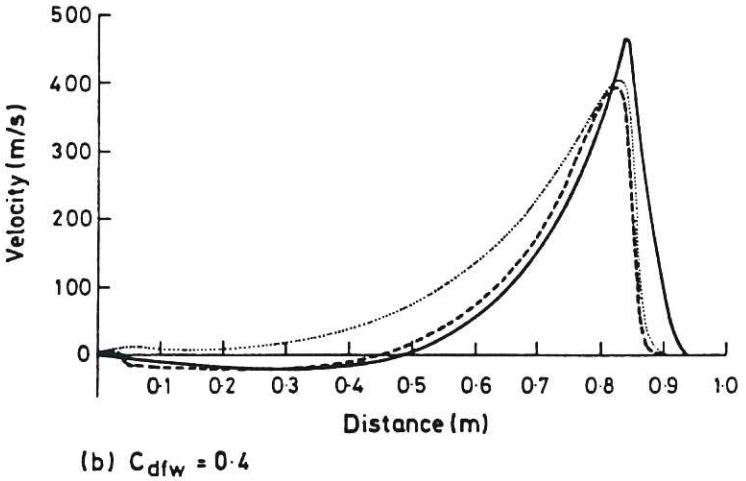

Figure 14: A comparison of the velocity fields for cases with and without slip between the fragment and water phases.